

The London moment was measured by rotating the disk-shaped superconductors inside a flux transformer which couples the magnetic flux to a commercial r.f. SQUID. All measurements were done by first cooling to 4.2 K and then setting the sample into rotation. This results in a signal that is proportional to the shielded volume fraction in a zero-field cooled magnetization measurement. A lead sample shaped as closely as possible to the same dimensions as the $\text{YBa}_2\text{Cu}_3\text{O}_{7-\delta}$ sample is used to calibrate the measurement. When inserting the free-electron mass and charge in equation (1) a magnetic field of $\omega \times 1.14 \times 10^{-11}$ T is expected, with ω in rad s^{-1} . With the measured self-inductance of the flux transformer and an estimate of the fraction of the flux actually detected, the intensity of the magnetic field measured for the lead sample is within 10% of this value. The 10% error is the result of uncertainties in the geometrical factors and the actual self-inductance of the flux transformer with the superconductor in the primary coil. This error only affects the absolute values. For the measurement on the high-temperature superconductors the lead sample serves as a reference.

Figure 1 shows that the magnetic moment varies linearly with frequency. The moment changes sign when the sense of rotation is reversed. The sign of the signals of the three samples is the same. From Fig. 1 it is clear that the signals of $\text{YBa}_2\text{Cu}_3\text{O}_{7-\delta}$ and Pb are equal, within the experimental error. For $\text{BaPb}_{0.8}\text{Bi}_{0.2}\text{O}_3$ the signal is about 25% smaller than that of the Pb reference sample. This may be attributed to the non-ideal shielding found for the $\text{BaPb}_{0.8}\text{Bi}_{0.2}\text{O}_3$ sample, and to slightly different sample dimensions. When corrections are applied for the coupling factor of the signal to the flux transformer and the signal is scaled to the measured shielded volume fraction, it is again equal to the Pb reference signal to within the estimated accuracy. We conclude that the abundance of defects and grain boundaries in our sintered high- T_c materials have no other effect on the London moment than to reduce it in proportion to the reduced shielding.

From these observations we conclude that the superconductivity in $\text{YBa}_2\text{Cu}_3\text{O}_{7-\delta}$ and $\text{BaPb}_{0.8}\text{Bi}_{0.2}\text{O}_3$ corresponds to a superfluid phase in the London sense. The value of the London moment is equal to that of conventional BCS superconductors. From this it follows in particular that the mass in equation (1) is the free-electron mass irrespective of the material. This last result is of some interest in view of the special nature of the oxide superconductors, which can be thought of as being derived from semiconductors by suitable doping or varying the oxygen concentration (self-doping). The conductivity in the normal state is associated with negatively charged carriers in $\text{BaPb}_{0.8}\text{Bi}_{0.2}\text{O}_3$ but with positive carriers (holes) in the case of $\text{YBa}_2\text{Cu}_3\text{O}_{7-\delta}$. Because of the low carrier densities and very small coherence lengths, it has been proposed (see, for example, refs 7, 8) that real-space pairing is the superconductivity mechanism, as opposed to the k -space (Cooper) pairing of the BCS theory. One might expect heavy masses for such carriers but this work demonstrates that the effective-mass concept is irrelevant for the London moment, that is, it involves the bare mass m_e irrespective of the nature of the carriers in the normal state. This may be understood from the fact that the London moment is a magneto-mechanical effect³ and therefore involves the true mechanical momentum $m_e v$ of the carriers (see also refs 4, 5). □

Three-dimensional twisted vortices in an excitable chemical medium

A. M. Pertsov, R. R. Aliev & V. I. Krinsky

Institute of Biophysics, USSR Academy of Sciences, 142292 Pushchino, Moscow Region, USSR

SEVERAL different types of three-dimensional nonlinear wave structure are expected to occur in chemically excitable media¹. In general these are vortex-like structures (Fig. 1, for example) in which the waves adopt complex spatial configurations (curved, knotted, twisted or closed into rings). But until recently only simple vortices and vortex rings have been observed experimentally, for example in the Belousov-Zhabotinsky (B-Z) reaction²⁻⁴ and in cardiac tissue⁵. Here we report a new type of structure, twisted vortices, observed in a B-Z reaction immobilized in agarose gel (Fig. 2). In cross-section, a twisted vortex resembles a rotating spiral with a phase of rotation that changes along the filament. The filament extends through the entire medium, terminating at its free surfaces. The wavelength of a twisted vortex is shorter than that of a simple one and decreases with increasing twist, in accord with theory^{6,7}. The period shows little dependence on twist, contrary to the results of computer experiments⁶. Twisted vortices decay into simple ones; their twist decays exponentially with a time constant that increases with filament length. These dynamics are consistent with the theory of diffusional untwisting^{8,9} rather than that of shock waves¹⁰.

In a three-dimensional excitable medium, simple vortices are formed readily (Fig. 1a). These are rotating spiral waves that represent a straightforward extension of those seen in two dimensions, the rotation phase being independent of the third coordinate. Most of the spiral waves observed experimentally (for example, in the B-Z reaction^{2-4,11,12}, in cardiac muscle¹³, in the retina¹⁴ and in slime molds¹⁵), are such simple three-dimensional vortices. But numerical experiments with a Fitz-Hugh-Nagumo model¹⁶ and analytical theory⁶ predict that twisted vortices should have smaller periods and wavelengths than other types of autonomous waves and thus should dominate over these by suppressing and expelling them.

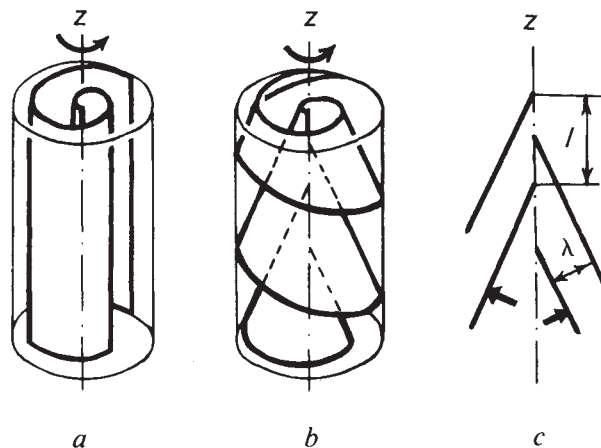


FIG. 1 Schematic representations of simple (a) and twisted (b, c) vortices. The top view of a twisted vortex is a rotating spiral wave. The side view comprises overlapping cones, seen in cross-section in c. The dash-dotted line is the rotation axis, and solid lines represent wave fronts. The directions of wave propagation and rotation are indicated by arrows. λ is the wavelength and l is the distance at which the phase shift is 2π . The twist $w = 2\pi/l$.

Received 7 March; accepted 18 April 1990.

- London, F. *Superfluids* Vol. 1 (Wiley, New York, 1950).
- Becker, R., Heller, G. & Sauter, F. *Z. Physik* **85**, 772-787 (1933).
- Broer, L. J. F. *Physica* **13**, 473-478 (1947).
- Cabrera, B., Gutfreund, H. & Little, W. A. *Phys. Rev.* **B25**, 6644-6654 (1982).
- Cabrera, B. & Peskin, M. E. *Phys. Rev.* **B39**, 6425-6430 (1989).
- Tate, J., Cabrera, B., Felch, S. B. & Anderson, J. T. *Phys. Rev. Lett.* **62**, 845-848 (1989).
- Micnas, R., Ranninger, J. & Robaszkiewicz, S. *Rev. Mod. Phys.* **62**, 113-171 (1990).
- de Jongh, L. J. *Physica* **C152**, 171-216 (1988); *Physica* **C161**, 631-655 (1989).

ACKNOWLEDGEMENTS. We thank J. M. J. van Leeuwen for his interest and for discussions. This investigation is part of the Dutch National Research Program on high-temperature superconductivity.

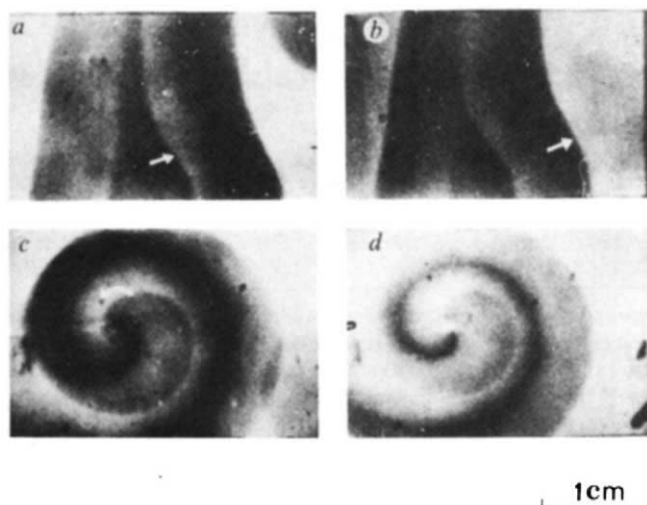


FIG. 2 A twisted vortex ($w=3\text{ cm}^{-1}$) in a chemically excitable medium. *a, b*, Side views (compare Fig. 1*c*); *c, d*, top views (compare Fig. 1*b*). The interval between *a* and *b*, and *c* and *d*, is 4 min. Arrows show the direction of wave propagation. Light is absorbed mostly by the portions of waves that lie perpendicular to the plane of the figure, so that in *a* and *b* only the central cross-section of the twisted vortex (Fig. 1*c*) is seen. The excitable medium is a B-Z reagent immobilized in agarose gel^{4,17,18}. The recipe was chosen to make photography of the thick layers possible: (50 mM NaBrO₃, 50 mM CH₂(COOH)₂, 150 mM H₂SO₄, 0.65 mM ferroin, 0.75% agarose.) The temperature is 20 °C.

We obtained twisted vortices from simple ones by creating temperature gradients along vortex filaments. Simple vortices with straight-line filaments were obtained by the standard method¹⁶. In the middle of a rectangular glass cuvette containing immobilized B-Z reagent, we placed a vertical plastic screen 0.1 mm thick, thus dividing the cuvette into two compartments. In one of these, a cylindrical wave was initiated by inserting a vertical thin silver wire. On reaching the screen, the wave broke along the generatrix (a line whose motion generates a surface) of the cylinder, the breaking edges corresponding to two straight lines which moved away from each other along the screen surface. When one of these reached the wall of the cuvette, the screen was removed and the other breaking edge curled into a simple scroll with a straight-line filament. A glass top was placed on the cuvette, so that both ends of the filament were in contact with glass, to avoid inhibition of the reaction by oxygen.

To obtain a twisted scroll the cuvette was placed on a thermostat-controlled stage heated above room temperature. This caused a local increase in the reaction rate and in the velocity of vortex rotation. An increase in temperature by 1 °C caused a decrease in the period from about 10 min to 0.5 min. These differences in local rotation velocities resulted in the development of a twist. For unequal angular frequencies of rotation, ω , the phase difference $\Delta\phi$ between two cross-sections perpendicular to the vertical (z -) axis grows linearly with time ($\Delta\phi = t\Delta\omega$), so vortices with different twists w ($w = d\phi/dz$) could be obtained by varying the time and heating temperature.

Figure 2 shows a twisted vortex. The top view corresponds to a rotating spiral wave, and the side view shows cones produced by the wave fronts. As the vortex rotates, the waves move from the centre (indicated by the arrow) to the periphery at a constant velocity.

We have studied the dependence of vortex characteristics on twist. The average twist w is defined as $w = 2\pi/l$ (see Fig. 1*c*); l was measured from the photographs. An increase in w causes a decrease in wavelength λ (Fig. 3*c*) and a weaker decrease in the rotation period (Fig. 3*b*). These are consequences of the dispersion relation for the B-Z reaction. Our measurements of the dispersion curve showed that a twist-induced change in

wavelength from 0.5 to 0.9 cm (as in Fig. 3*c*) corresponds to a slow change in rotation period from 9.0 to 10.5 min (similar to Fig. 3*b*).

When the twist exceeds a critical value w_c ($\approx 7\text{--}9\text{ cm}^{-1}$), the regular rotation of the twisted vortex is disturbed and breaks in the wave occur (arrow in Fig. 3*a*). Further increases in w give rise to a pattern resembling turbulence¹⁹. There exists a minimum wavelength for a stable wave, λ_{\min} , which can be estimated from the dispersion relation ($\lambda_{\min} \approx 0.45\text{ cm}$); λ_c is found to be close to this value.

In theory, vortices with twists below the critical value should evolve into simple ones. Spontaneous untwisting of a twisted vortex was first demonstrated in numerical experiments⁷. Analytical theories⁸⁻¹⁰, however, predict different untwisting kinetics. The theory of shock waves, based on the first-order differential equation $w_t = \omega_w w_z$, states that the wave of untwisting propagates with velocity ω_w along the twisted vortex¹⁰. A more accurate equation describing the evolution of a

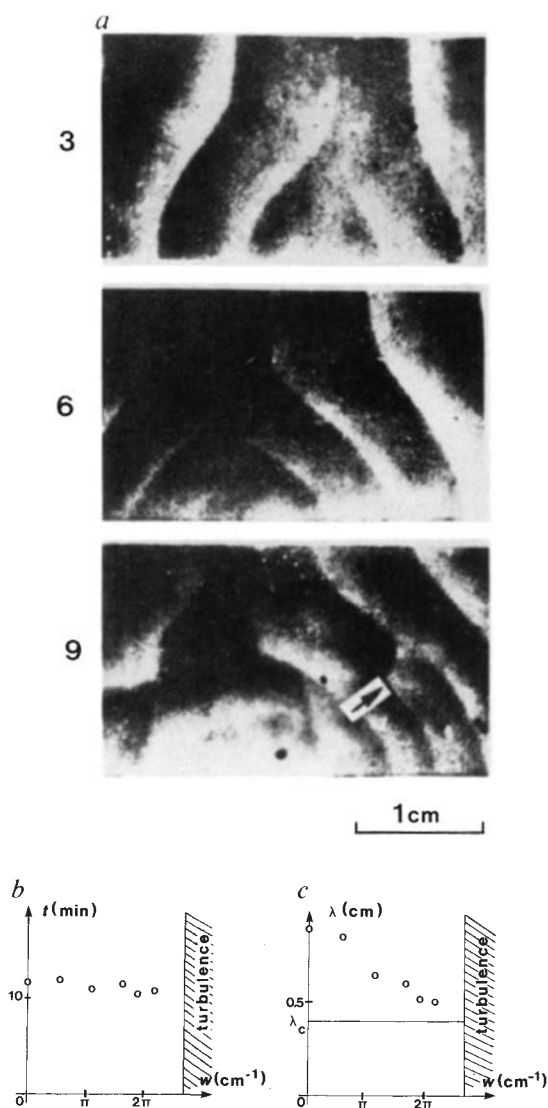


FIG. 3 Twisted vortices with different twists. *a*, Side views (compare Fig. 2*a, b*). Numbers on the left denote the average twist w in cm^{-1} . At $w=9\text{ cm}^{-1}$ a wave break is seen (arrow). *b, c*, Dependence of rotation period T and wavelength λ on twist w . T and λ were measured when the maximum temperature variation within the cuvette (measured with MT54M microthermistors) was no greater than 0.15 °C. The errors in the vortex rotation periods due to residual temperature gradients do not exceed 1%.

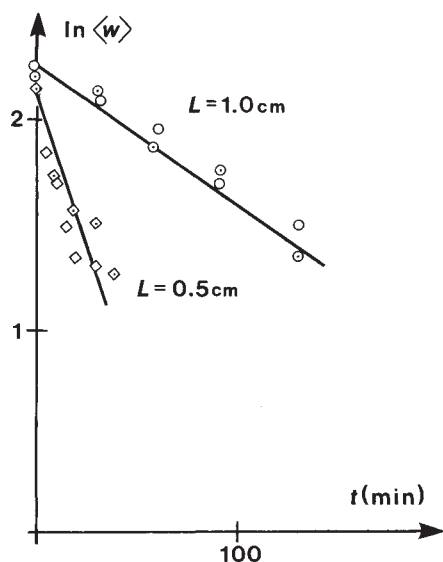


FIG. 4 Evolution of twist w . For sample thicknesses $L=1.0$ and 0.5 cm, the kinetics of untwisting are seen to be exponential. Two sets of data are shown for each thickness. A least-squares fitting of the straight lines gives time constants τ as 161 min and 45 min respectively.

twist was proposed in ref. 8:

$$w_t = \omega_w w_z + Dw_{zz} \quad (1)$$

Solution of this equation for $\omega_w = \text{constant}$ and boundary conditions $W_z|_{z=0,L}=0$ (where L is the cuvette length) predicts exponential untwisting:

$$w(t) \propto \exp(-t/\tau); \tau = (D\pi^2/L^2 + \omega_w^2/4D)^{-1} \quad (2)$$

Our experiments confirm that vortices with twists below the critical value transform to simple ones. Moreover, the kinetics of untwisting were found to be exponential (Fig. 4) and at variance with the simple shock-wave theory of ref. 10; the time constant τ increases with L .

Equation (2) fits our experiments qualitatively but not quantitatively. Equation (2) predicts that τ is proportional to L^2 at small L . We found that a twofold increase in L (from $L=0.5$ cm to 1 cm) indeed resulted in about a fourfold increase in τ (see Fig. 4 legend), but further increase in L (from 1 cm to 2 cm) increased τ by about a factor of seven. This remains to be explained theoretically. □

Received 15 September 1989; accepted 20 March 1990.

1. Winfree, A. T. & Strogatz, S. H. *Nature* **311**, 611–615 (1984).
2. Winfree, A. T. *Science* **181**, 937–939 (1973).
3. Welsh, B., Gomatam, S. & Burgess, A. *Nature* **304**, 611–614 (1983).
4. Jahnke, W., Henze, C. & Winfree, A. *Nature* **336**, 662–665 (1988).
5. Medvinsky, A. B., Panfilov, A. V. & Pertsov, A. M. in *Self-Organization. Autowaves and Structures Far from Equilibrium* (ed. Krinsky, V.) 195–199 (Springer, Berlin, 1984).
6. Mikhailov, A. S., Panfilov, A. V. & Rudenko, A. N. *Phys. Lett. A* **109**, 246–250 (1985).
7. Panfilov, A. V., Rudenko, A. N. & Pertsov, A. M. *Dokl. Akad. Nauk SSSR* **279**, 1000–1002 (1984).
8. Biktashev, V. N. *Physica D* **36**, 167–172 (1989).
9. Keener, J. P. *Physica D* **31**, 269–276 (1988).
10. Braznik, P. K., Davydov, V. A., Zykov, V. S. & Mikhailov, A. S. *Abstr. 2nd All-Union Conference on Mathematical and Computational Methods* 118–119 (ONTI NCBI, Pushchino, 1987).
11. Zhabotinsky, A. M. & Zaikin, A. N. in *Oscillatory Processes in Biological and Chemical Systems* Vol. 2, 279–283 (ONTI NCBI, Pushchino, 1971).
12. Agladze, K. I. & Krinsky, V. I. *Nature* **296**, 424–426 (1982).
13. Allesio, M. A., Bonke, F. I. M. & Schopman, F. J. G. *Circul. Res.* **33**, 54–62 (1973).
14. Bures, J. & Gorelova, N. A. *J. Neurobiol.* **14**, 353–363 (1983).
15. Gerish, G. *Curr. Topics devl. Biol.* **3**, 157 (1968).
16. Panfilov, A. V. & Pertsov, A. M. *Dokl. Akad. Nauk SSSR* **274**, 1000–1002 (1984).
17. Kuhnert, L. *Naturwissenschaften* **70**, 464–466 (1983).
18. Nosztzcius, Z., Hopfthornke, W., McCormick, W. D., Swinney, H. L. & Tam, W. Y. *Nature* **329**, 619–620 (1987).
19. Agladze, K. I., Krinsky, V. I. & Pertsov, A. M. *Nature* **308**, 834–835 (1984).

ACKNOWLEDGEMENTS. We thank K. I. Agladze and V. N. Biktashev for helpful discussions.

Microbially mediated cerium oxidation in sea water

James W. Moffett

Chemistry Department, Woods Hole Oceanographic Institution, Woods Hole, Massachusetts 02543, USA

REDOX processes influence the geochemistry of many elements in the ocean, but attributing the distribution of these elements in the water column and sediments to specific redox processes is difficult because they are also influenced by non-redox processes and by other inputs that are poorly constrained. Cerium provides an opportunity to study redox processes in the ocean^{1–5} because its redox chemistry leads to its enrichment or depletion ('cerium anomalies') with respect to its lanthanide neighbours. A detailed understanding of Ce geochemistry is lacking, however, because of the paucity of knowledge of the redox rates and mechanisms in natural waters. Here I report measurements of Ce(III) oxidation rates using radiotracers in seawater samples collected in the Sargasso Sea and in Vineyard Sound, Massachusetts, which are much faster than previous, indirect estimates¹. The data indicate that the negative Ce anomaly in sea water is the result of microbial oxidation followed by preferential scavenging of Ce(IV); no abiotic oxidation was detectable. This suggests that inhibition by sunlight of microbial oxidation and scavenging of Ce and Mn contribute to the pronounced surface maxima observed for these elements.

Current knowledge of cerium redox chemistry in natural waters has been inferred from its distribution in the water column and various mineral phases, and from thermodynamic data in the literature^{1–5}. These indicate that Ce is preferentially removed from oxic waters by oxidation to insoluble Ce(IV), the thermodynamically stable form. Manganese oxide phases, such as Mn nodules, are strongly enriched in Ce (refs 2, 6), indicating that oxidation on Mn oxides may be a mechanism for Ce removal. The similarity of Ce and Mn marine geochemistry is also consistent with this hypothesis. But it is not clear if this similarity arises because of Ce oxidation on Mn oxides or because the distributions of both elements are controlled by common processes. Existing data provide no information on the timescales of the redox transformations of Ce, essential for complete understanding of its geochemistry and usefulness as a redox tracer.

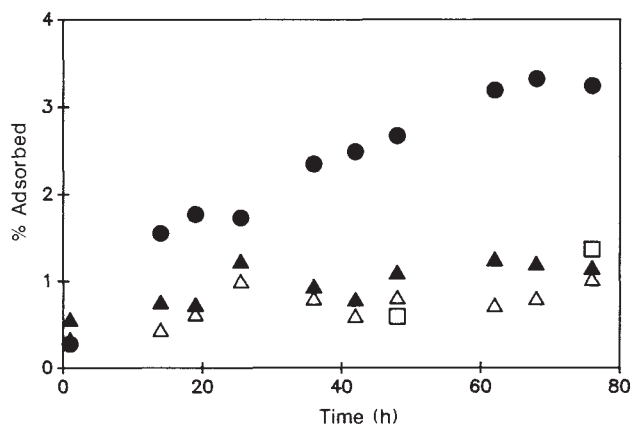


FIG. 1 Fraction of added radiotracer adsorbed on 0.2- μm -filterable particles for a sample collected at 120 m in the Sargasso Sea ($32^{\circ}16'N$, $64^{\circ}36'W$). Samples were collected in Teflon-coated bottles on Kevlar wire and processed within 2 h of collection. All samples were incubated in the dark, at 25 $^{\circ}\text{C}$ in 2-l polycarbonate bottles. Adsorption of tracers on container walls was negligible. Filters counted in NaI detector. Absolute precision = $\pm 0.2\%$. ●, ^{139}Ce ; ▲, $^{139}\text{Ce} + 1 \text{ g l}^{-1}$ azide (added to entire sample 1 h before tracer addition); □, $^{139}\text{Ce} + 10^{-4} \text{ M}$ ascorbate (ascorbate solution, pH 8, added to each aliquot 1 h before filtration); △, ^{152}Eu .